Targeting Amyloid Formation of Proteins Through Surface Functionalized Nanoparticles

Over the past decade, strategically synthesized nanoparticles (NPs) with potential drugs have earned great interest to target several medical complications including amyloid formation of proteins. The process of amyloid formation of proteins is known to be associated with several pathologies, including many neurodegenerative diseases. One of the approaches to target amyloid linked diseases and their associated medical severities is to find potential inhibitors against the onset of amyloid formation of proteins.

Here, in this chapter using a combination of biophysical methods, inhibition effect of tyrosine coated gold nanoparticles (AuNPs^{Tyr}), tyrosine coated silver nanoparticles (AgNPs^{Tyr}) and tryptophan coated gold nanoparticles (AuNPs^{Trp}) on amyloid formation of insulin has been studied.

5.1 EFFECT OF AuNPs^{Tyr} and AuNPs^{Trp} ON INSULIN AMYLOID FORMATION

Hydrophobic residues including aromatic amino acids are known to play a key role during amyloid formation of proteins, via intermolecular hydrophobic interactions (Chiti and Dobson 2009) (Fandrich, Fletcher et al. 2001). Hence adapting strategies that interfere with the intermolecular hydrophobic interactions, by targeting exposed hydrophobic groups, may possibly provide an effective approach to inhibit such aggregation process. In accordance with this hypothesis, in this work metallic nanoparticles surface functionalized with selected hydrophobic residues (Tyrosine and Tryptophan) were synthesized, and these NPs were studied against amyloid formation of proteins, considering insulin as a convenient model system.

5.1.1 Characterization of Tyrosine and Tryptophan Coated Metal NPs

Gold nanoparticles coated with tyrosine (AuNPs^{Tyr}) and tryptophan (AuNPs^{Trp}), and silver nanoparticles coated with tyrosine (AgNPs^{Tyr}) were synthesized by an established protocol (Selvakannan 2013)] (see Annexure A). Schematic representations of these NPs are shown in Figure 5.1a. UV-visible absorption spectroscopy was primarily employed to confirm the existence of stable metal nanoparticles by obtaining characteristic signature curves of Surface Plasmon Resonance (SPR) absorption bands. UV visible spectra of the synthesized nanoparticles are shown in Figure 5.1b, where SPR absorbance peak of AuNPs^{Tyr} and AgNPs^{Tyr} samples were obtained at ~523 nm and ~417 nm respectively, wherein the SPR absorbance peak of AuNPs^{Trp} sample was at ~525 nm. The acquired SPR absorption curves of AuNPs^{Tyr}, AuNPs^{Trp} and AgNPs^{Tyr} samples were in accordance with the reported values for similar nanoparticles. FTIR spectroscopic analysis of all the synthesized NPs, as described in Figure 5.1c, provides a direct evidence of amino acids interaction with the nanoparticles. In FTIR data a shift in the carbonyl stretching frequency of tryptophan was recorded from *1666 cm^{-1} (—) to 1707 cm^{-1} for AuNPs^{Trp} (—) sample and carbonyl stretching frequency of tyrosine was around *1610 cm^{-1} (—), which was shifted to 1740 cm^{-1} for AuNPs^{Tyr} and AgNPs^{Tyr} (— and —) nanoparticles. Transmission electron micrographs (TEM) of AuNPs^{Tyr}, AuNPs^{Trp} and AgNPs^{Tyr} samples were shown in Figure 5.1d. Here, TEM images were analyzed by imageJ software and all nanoparticles appeared spherical with a uniform diameter of ~10-30 nm, Figure 5.1e.
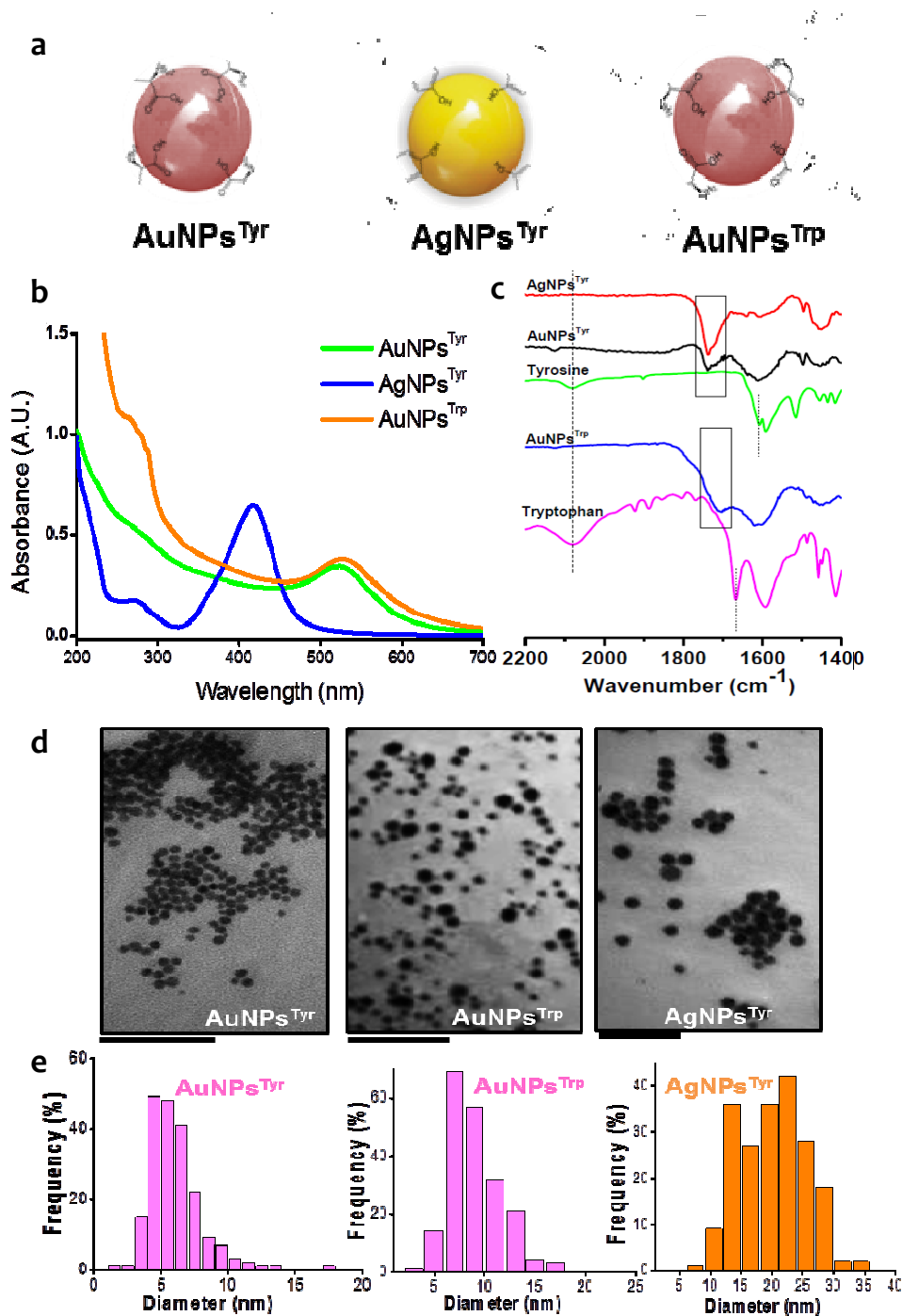
Figure 5.1 : Characterization of tyrosine and tryptophan cappeed nanoparticles. (a) Schematic representing tyrosine (AuNPs^{Tyr}and AgNPs^{Tyr}) and tryptophan (AuNPs^{Trp}) coated nanoparticles. The orientation of the attached tyrosine residues over the silver nanoparticles (AgNPs^{Tyr}) was kept reversed as compared to AuNPs^{Tyr}. (b) UV-visible spectra of the nanoparticle samples: (—) AuNPs^{Tyr}; (—) AuNPs^{Trp}; and (—) AgNPs^{Tyr}. (c) FTIR spectra of nanoparticles samples: (—) AgNPs^{Tyr}; (—) AuNPs^{Tyr}; (—) Tyrosine; (—) AuNPs^{Trp}; and (—) Tryptophan. (d) Transmission electron microscopic images of AuNPs^{Tyr}, AuNPs^{Trp} and AgNPs^{Tyr}. Scale bar, 100 nm. The average diameter of the nanoparticles was observed around ~10-30 nm. (e) Particles size histograms corresponding to tyrosine and tryptophan coated AuNPs^{Tyr}, AuNPs^{Trp} and AgNPs^{Tyr} nanoparticles. This analysis was done by using ImageJ software.

5.1.2. Effect of Surface Functionalized NPs on Insulin Amyloid Formation

Further, these synthesized NPs were tested, for their antiamyloid efficacies, against amyloid formation process using insulin as a model system. Temperature induced amyloid formation of insulin was studied in physiological buffer at temperature, ~70°C, which is close to the melting temperature (T_m) of insulin. The aggregation process was recorded by monitoring the rise in the Thioflavin T signal at different time points, as shown in Figure 5.2.
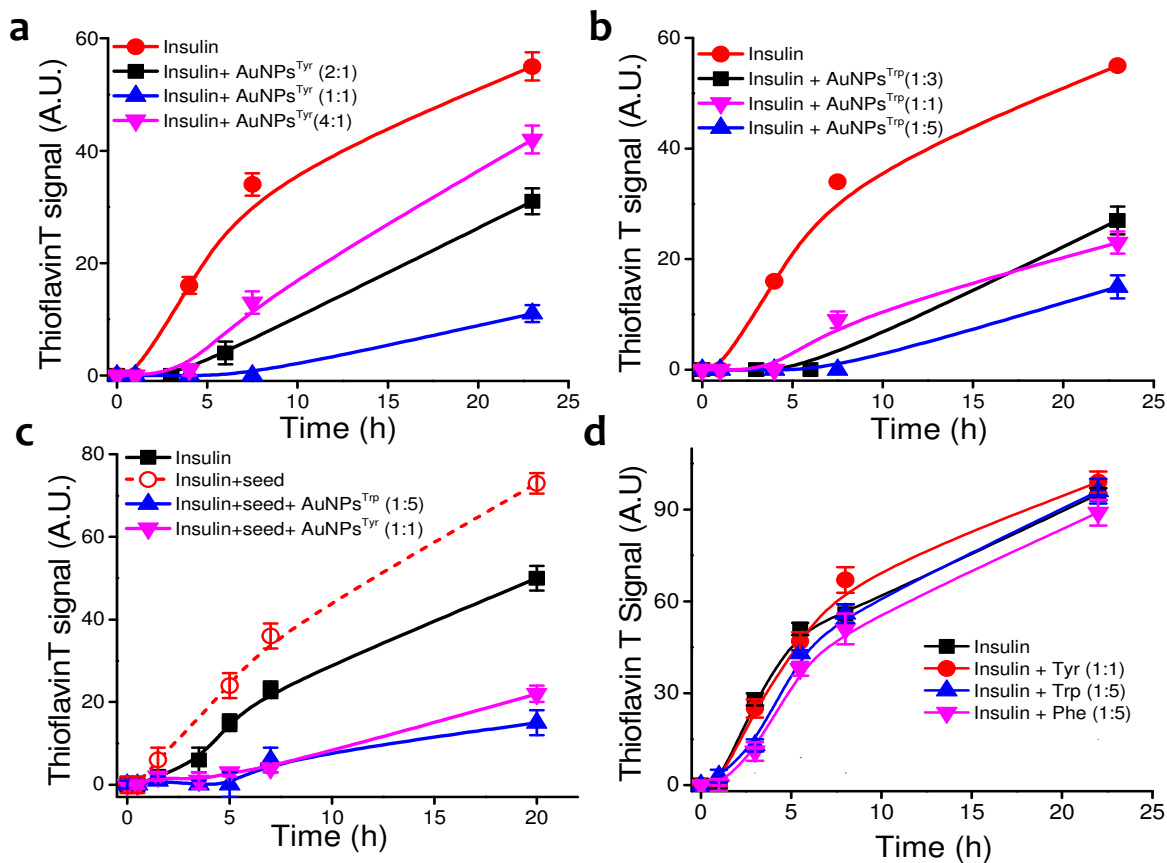

Figure 5.2 : Inhibition of insulin amyloid formation by tyrosine and tryptophan coated nanoparticles. (a) Effect of AuNPs[Tyr] on aggregation of ~40 µM insulin sample at different values of molar ratio: (●) Insulin; (▼) Insulin + AuNPs[Tyr] at 4:1; (■) Insulin+ AuNPs[Tyr] at 2:1; (▲) Insulin+ AuNPs[Tyr]at 1:1. (b) Effect of AuNPs[Trp] on spontaneous aggregation of ~40 µM insulin at different molar ratios: (●) Insulin only; (▼) Insulin+ AuNPs[Trp] at 1:1 molar ratio; (■) Insulin+ AuNPs[Trp] at 1:3 molar ratio; (▲) Insulin+ AuNPs[Trp] at 1:5 molar ratio.(c) Effect of AuNPs[Tyr] and AuNPs[Trp] on seed-induced aggregation of insulin (■) Insulin only; (O) Insulin+ 15% (w/w) seed; (▼) Insulin+seed+AuNPs[Tyr] at 1:1 molar ratio; (▲) Insulin+seed+AuNPs[Trp] at 1:5 molar ratio. (d) Effect of isolated tyrosine, tryptophan and phenylalanine residues on aggregation of insulin: (■) Insulin only; (●) Insulin+ Tyr at 1:1; (▲) Insulin+ Trp at 1:5; (▼) Insulin+Phe at 1:5 molar ratio.

A characteristic aggregation curve comprising of a distinct lag phase, a growth phase and a saturation phase was obtained when soluble insulin monomers at ~40 µM was incubated (Figure 5.2,●) under aggregating condition. Final aggregates of insulin showed typical amyloid morphology when examined under TEM (Figure 5.3d) as seen in the previous studies (Krebs, Morozova-Roche et al. 2004). The inhibition effect of amino acid coated nanoparticles was examined at three different molar ratio values (of insulin:inhibitor) as mentioned in Figure 5.2. Both AuNPs[Tyr] and AuNPs[Trp] showed dose dependent inhibition of insulin amyloid formation (Figure 5.2a and 5.2b). Further, isolated aromatic residues (phenylalanine, tyrosine and tryptophan) were tested on amyloid formation of insulin, to confirm the inhibitory effect of coated NPs with tyrosine and tryptophan residues. The data as shown in Figure 5.2d clearly indicate that insulin alone and the amino acid treated insulin samples showed similar kinetics

during amyloid formation. This result confirms that tyrosine and tryptophan molecules are effective in inhibiting the amyloid formation of insulin only when they are attached to the surface of the nanoparticles. The inhibition effect of AuNPs^{Tyr} was found to be slightly more suppressing than the effect observed for AuNPs^{Trp} at similar concentration (Figure 5.2a, ▲ and 5.2b, ▼).

Next, seed-induced aggregation of insulin was performed to know the effect of the synthesized nanoparticles on the behavior of mature amyloid fibrils of insulin. Here, when insulin monomers were incubated in the presence of seeds (~15% w/w), a rapid rise in the Thioflavin T signal was observed without any lag phase. However seed-induced aggregation of insulin was inhibited in the presence of AuNPs^{Tyr} (Figure 5.2c, ▼) and AuNPs^{Trp} (Figure 5.2c, ▲) nanoparticles. It appears that these nanoparticles have the ability to interfere with the recruitment of the monomers by mature fibrils which in turn suppresses the seeded elongation during aggregation process. To further clarify the interaction between the AuNPs^{Tyr} and mature fibrils, dissociation of insulin amyloid fibrils were examined against the synthesized nanoparticles.

To conduct disassembly experiments, AuNPs^{Tyr} sample was added to a suspension of mature insulin fibrils and Thioflavin T signal of the sample was monitored at different time intervals. The data shown in Figure 5.3f clearly indicate that AuNPs^{Tyr} promote disassembly of insulin amyloid fibrils. After ~240 hr of incubation time ~50% decrease of the initial Thioflavin T signal was observed (Figure 5.3f, ●), which suggests a substantial amount of fibril-dissociation in the presence of AuNPs^{Tyr}. In a previous study it has been reported that albumin modified magnetic fluid can cause the depolymerization of insulin amyloid fibrils (Siposova, Kubovcikova et al. 2012).

5.1.3. Effect of Surface Functionalized NPs on Conformational Properties of Insulin

Since both AuNPs^{Tyr} and AuNPs^{Trp} showed their potential either to inhibit or to interfere with amyloid formation of insulin, circular dichroism (CD) spectroscopy was employed to further understand whether these nanoparticles have any effect on the conformational properties of insulin or not. To answer this issue, first, the CD spectra of the insulin in the presence and in the absence of nanoparticles were obtained. The molecular conformation of insulin did not change in the presence of nanoparticles (Figure 5.3b). Next, thermal unfolding of insulin in PBS was recorded by monitoring the change in the CD signal at ~222 nm. The thermal unfolding curves showed no significant change in the T_m values of insulin samples in the presence of these nanoparticles (Figure 5.3a, □, O and ▷). These data suggest that molecular stability of the protein is not altered in the presence of NPs.

To understand the changes in the secondary structures of insulin during aggregation process, the CD signal of aggregating insulin samples in the presence of and in the absence of both AuNPs^{Tyr} and AuNPs^{Trp} was recorded at different time intervals, as shown in Figure 5.3c. Data clearly indicate that the process of conversion of native insulin molecules into β-structured species is delayed in the presence of nanoparticles (Figure 5.3c, — and —). Thioflavin T readings of the same samples were almost consistent with the CD data (Inset of Figure 5.3c), observed at different time-intervals (at 0hr and after 9 hr).
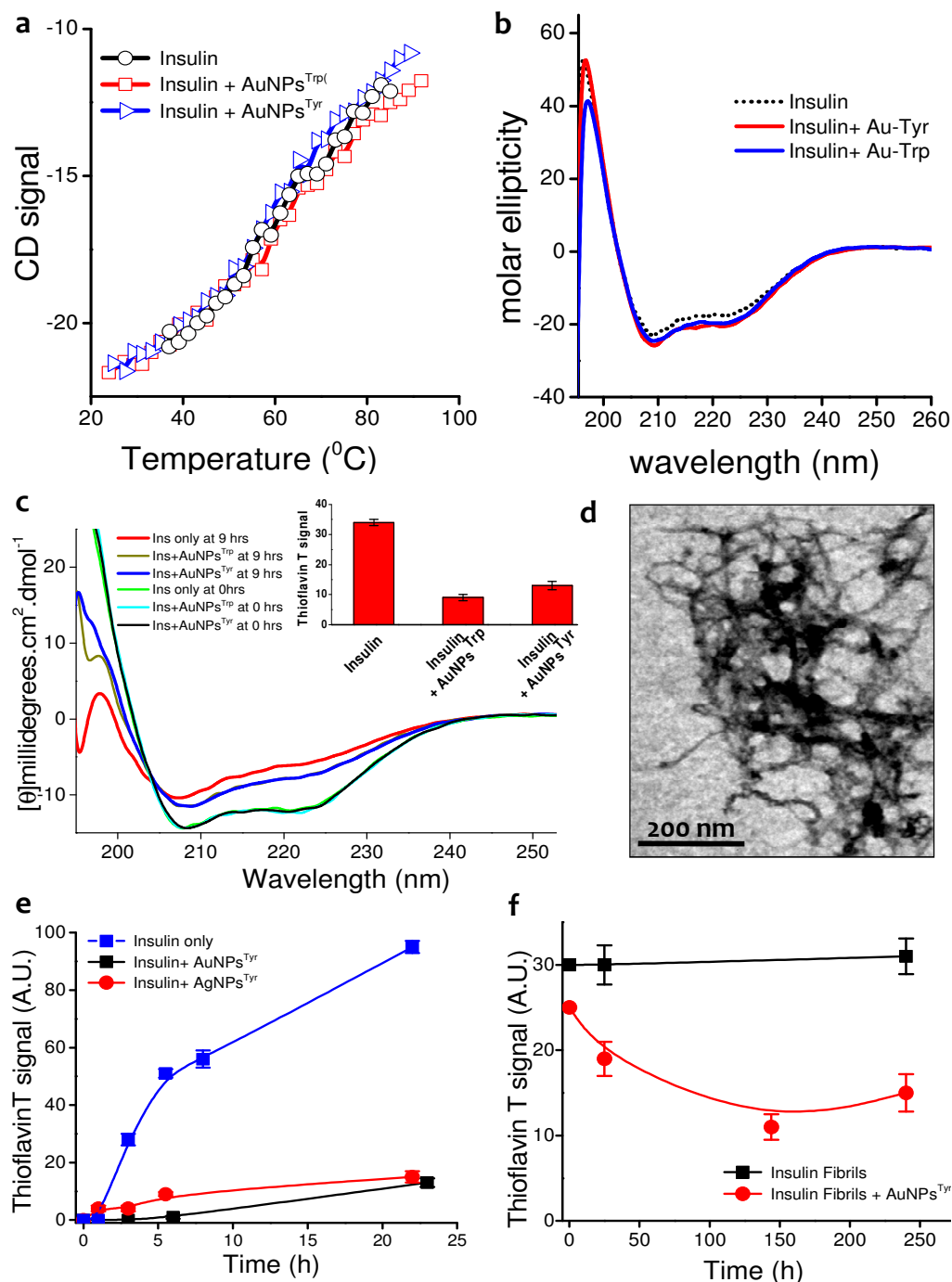
Figure 5.3 : (a) Thermal unfolding of insulin by circular dichroism by monitoring change of CD signal at ~222nm: (○) insulin only; (□) insulin+ AuNPs^{Tyr} at 1:1 ratio; (▷) insulin+ AuNPs^{Trp} at 1:5 molar ratio. (b) CD spectra of insulin in the presence and absence of Trp and Tyr coated nanoparticles: (······) insulin only; (—) insulin+ AuNPs^{Tyr} at 1:1 molar ratio; (—) insulin+ AuNPs^{Trp} at 1:5 molar ratio. (c) CD spectra of insulin undergoing aggregation in the presence and in the absence of nanoparticles: insulin only at 0 hr; (—) and 9 hr (—); insulin+ AuNPs^{Tyr} at 1:1 molarratio at 0 hr (—) and at 9 hr (—); insulin+ AuNPs^{Trp} at 1:1 molar ratio at 0 hr (—) and at 9 hr (—). Inset shows ThT signal of the CD samples at 9hrs. (d) TEM image of insulin mature amyloid fibrils. (e) Comparison of the effect of AuNPs^{Tyr} and AgNPs^{Tyr} on spontaneous aggregation of ~43 μM insulin: (■) insulin only; (●) insulin + AgNPs^{Tyr} at 1:1 molar ratio; (■) insulin + AuNPs^{Tyr} at 1:1 molar ratio.(f) Effect of tyrosine coated nanoparticles on disassembly of mature amyloid fibrils of insulin: (■) insulin fibrils; (●) insulin fibrils + AuNPs^{Tyr} at 1:1 molar ratio of insulin: tyrosine.

5.1.4. Molecular Docking Studies on Tyrosine-Insulin Interaction

Molecular docking studies between insulin and tyrosine were carried out to understand the molecular-level interactions between them, which might be one of the reasons behind the observed inhibition effect of NPs.

Blind docking studies (see Annexure A) were employed to predict a viable tyrosine-insulin interaction at a site within insulin's B-chain which spans from Val18–Arg22. The value of CDocker energy for the best pose (as shown in Figure 5.4a) was -29.02 kcal.mol^{-1} and its corresponding interaction energy was observed to be -22.95 kcal.mol^{-1}. Such energy values suggest the formation of a stable protein-ligand complex. Obtained tyrosine-insulin complex as shown in Figure 5.4a displays seven interactions comprising of four hydrogen bonds (B:ARG22:HE−L-tyrosine:O14, B:ARG22:HH21−L-tyrosine:O14, B:GLU21:OE1−L-tyrosine:H21, B:VAL18:O−L-tyrosine:H24), two pi interactions (B:GLU21:HN−L-tyrosine, B:GLY20:HA1−L-tyrosine) and one electrostatic bond (B:GLU21:OE2−L-tyrosine:N13). The stability of insulin-tyrosine complex was further ascertained using molecular dynamics study. Both root mean square deviation and total energy of the complex indicated the formation of a stable conformation after 5000 ps, Figure 5.5a and 5.5b. These data suggest that tyrosine's docking site spans from Val18 – Arg22 region of insulin's chain B and binding of tyrosine to that region of insulin may perhaps result in a stable protein-ligand complex. Further, some other docking studies were performed, on insulin-alanine and insulin-tryptophan, to understand the specificity of tyrosine-insulin interaction. The obtained data, Figure 5.6a and 5.6b, suggest that the number of hydrogen bonds formed between ligand and the protein was highest when the ligand was tyrosine and was lowest when the ligand was alanine. Further the molecular dynamics studies of tyrosine-insulin complex formation predict a more favourable complex in terms of energy and RMSD than that of insulin-alanine and insulin-tryptophan interactions, Figure 5.5a and 5.5b.

a   **b**
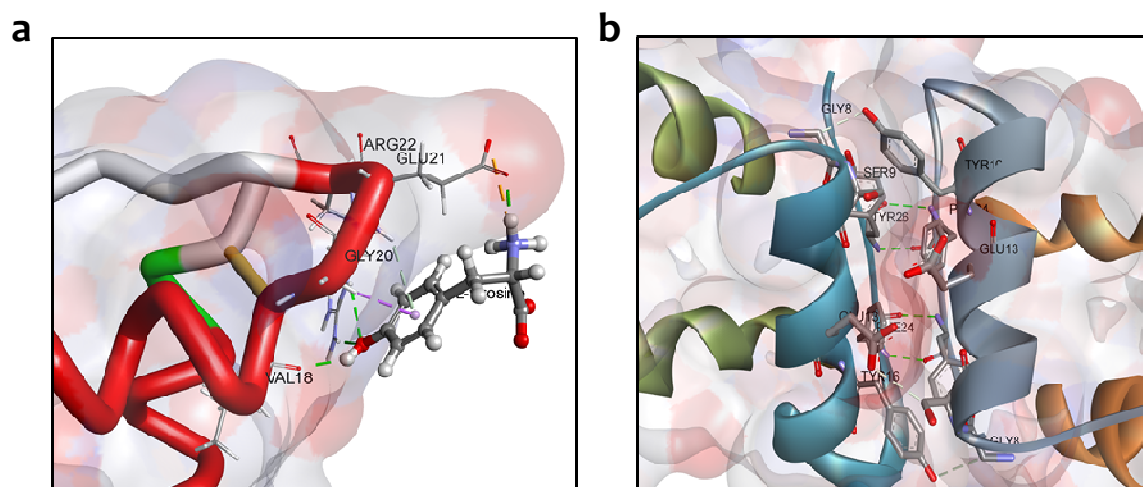
Figure 5.4 : (a) Molecular docking of a tyrosine molecule with insulin. The complex shows seven interactions comprising of four hydrogen bonds (B:ARG22:HE—L-tyrosine:O14, B:A RG22:HH21—L-tyrosine:O14, B:GLU21:OE1—L-tyrosine:H21, B:VAL18:O—L-tyrosine:H24), two pi interactions (B:GLU21:HN—L-tyrosine, B:GLY20:HA1—L-tyrosine) and one electrostatic bond (B:GLU21:OE2—L-tyrosine:N13). (b) Analysis of a crystal structure of insulin dimer to visualize the binding partners of tyrosine residue of one insulin molecule with different functional groups of another insulin molecule at the interface region. Discovery Studio 4.0 was used for the docking studies.
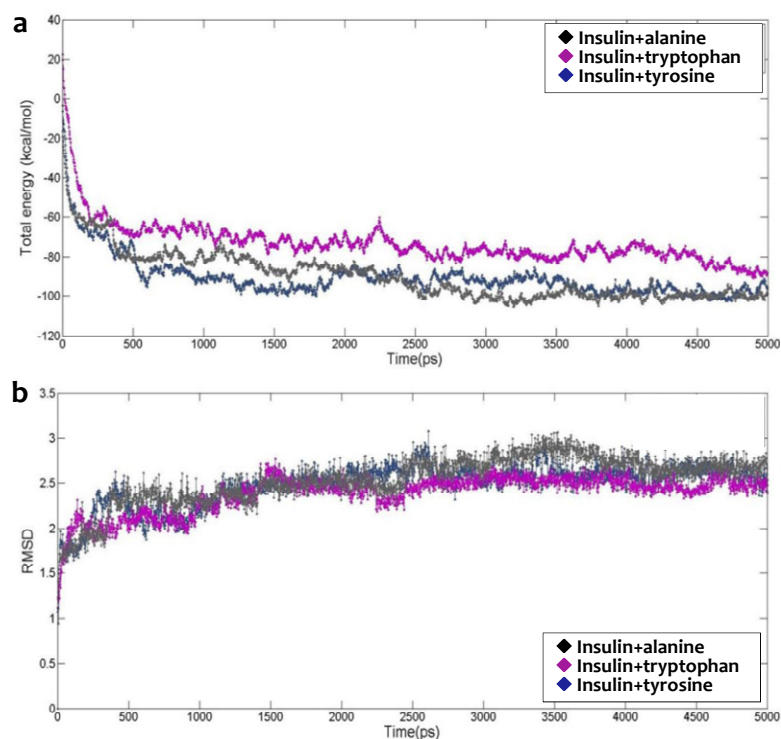
Figure 5.5 : Molecular dynamics studies on (◆)insulin-alanine, (◆) insulin-tryptophan and (◆) insulin-tyrosine docked complexes. (a) Energy vs time graph showing the stability of complexes over 5000 picoseconds, where tyrosine-insulin complex was found to be more stable. (b) RMSD vs time graph of the docked complexes. Discovery Studio 4.0 was used for the molecular docking studies.
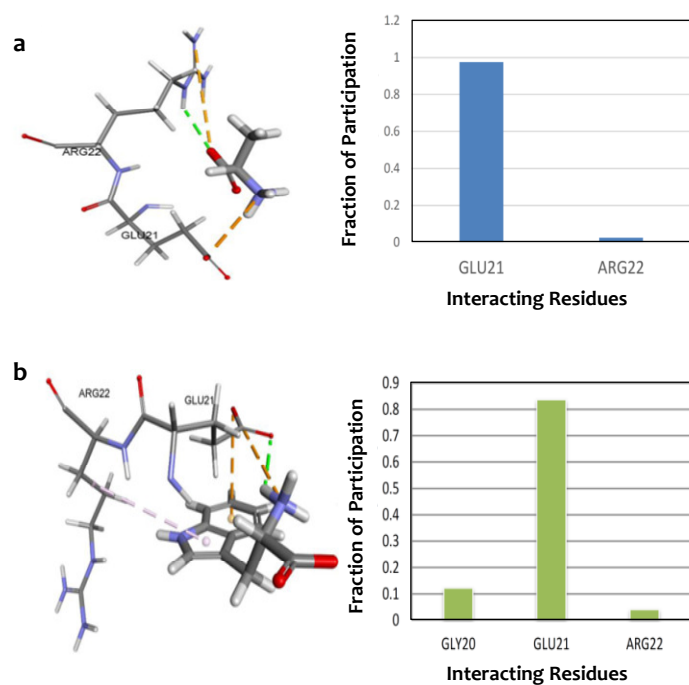
Figure 5.6 : Molecular docking studies, represents interaction complexes of: (a) alanine-insulin (CDocker energy= -23.4018 and Interaction energy= -14.0875 Kcal/mol); and (b) tryptophan-insulin (CDocker energy= -23.93 and Interaction energy= -17.0 Kcal/mol). Histogram represents fraction of participation of all the protein residues involved while making the interactions with ligand. Fraction of participation was calculated for all the amino acids participating in bond formation, when best 50 poses of ligand is docked with the insulin molecule.

To further clarify the possible binding partners of a tyrosine residue when it interacts with insulin, the available crystal structures of insulin dimers (PDB IDs: 2A3G, 2INS, 2ZP6, and 4IDW) (Smith, Duax et al. 1982; Smith, Pangborn et al. 2005; Margiolaki, Giannopoulou et al. 2013) were thoroughly analyzed. The interface of insulin-insulin dimers was examined to study the involvement of tyrosine residues during intermolecular interactions takes place when dimers were formed. Tyr16–Tyr26 region of chain B of insulin was found to be mediating important H-bonding interactions with average hydrogen bond length of 3.055 Å. Further data analysis clearly indicates that tyrosine residues are playing a key role during insulin-insulin dimer formation, Figure 5.4b and 5.7–5.11.

Name	Distance	Category	Type
B:PHE24:N - D:TYR26:O	2.92638	Hydrogen Bond	Conventional Hydrogen Bond
B:TYR26:N - D:PHE24:O	2.74485	Hydrogen Bond	Conventional Hydrogen Bond
B:TYR26:O - D:PHE24:N	3.03482	Hydrogen Bond	Conventional Hydrogen Bond
B:PHE24:O - D:TYR26:N	2.8752	Hydrogen Bond	Conventional Hydrogen Bond
B:GLY8:CA - D:TYR16:OH	3.46539	Hydrogen Bond	Carbon Hydrogen Bond
B:GLY23:CA - D:TYR26:O	3.05588	Hydrogen Bond	Carbon Hydrogen Bond
B:TYR16:OH - D:GLY8:CA	3.37682	Hydrogen Bond	Carbon Hydrogen Bond
B:GLU13:OE1 - D:SER9:CB	3.32819	Hydrogen Bond	Carbon Hydrogen Bond

Figure 5.7 : Analyzing molecular interactions of insulin dimer (PDB ID: 2A3G). (a) Represents interface of insulin dimer, where two insulin monomers are interacting by their B-chains via H-bonds. (b) Represents all the amino acid residues that are taking part in making H-bonds to stabilize the insulin dimer. (c) Represents all the details of the molecular interaction taking place such as, atoms that are taking part in bond formation, residues taking part, chain of insulin involved, bond length and type of bond.

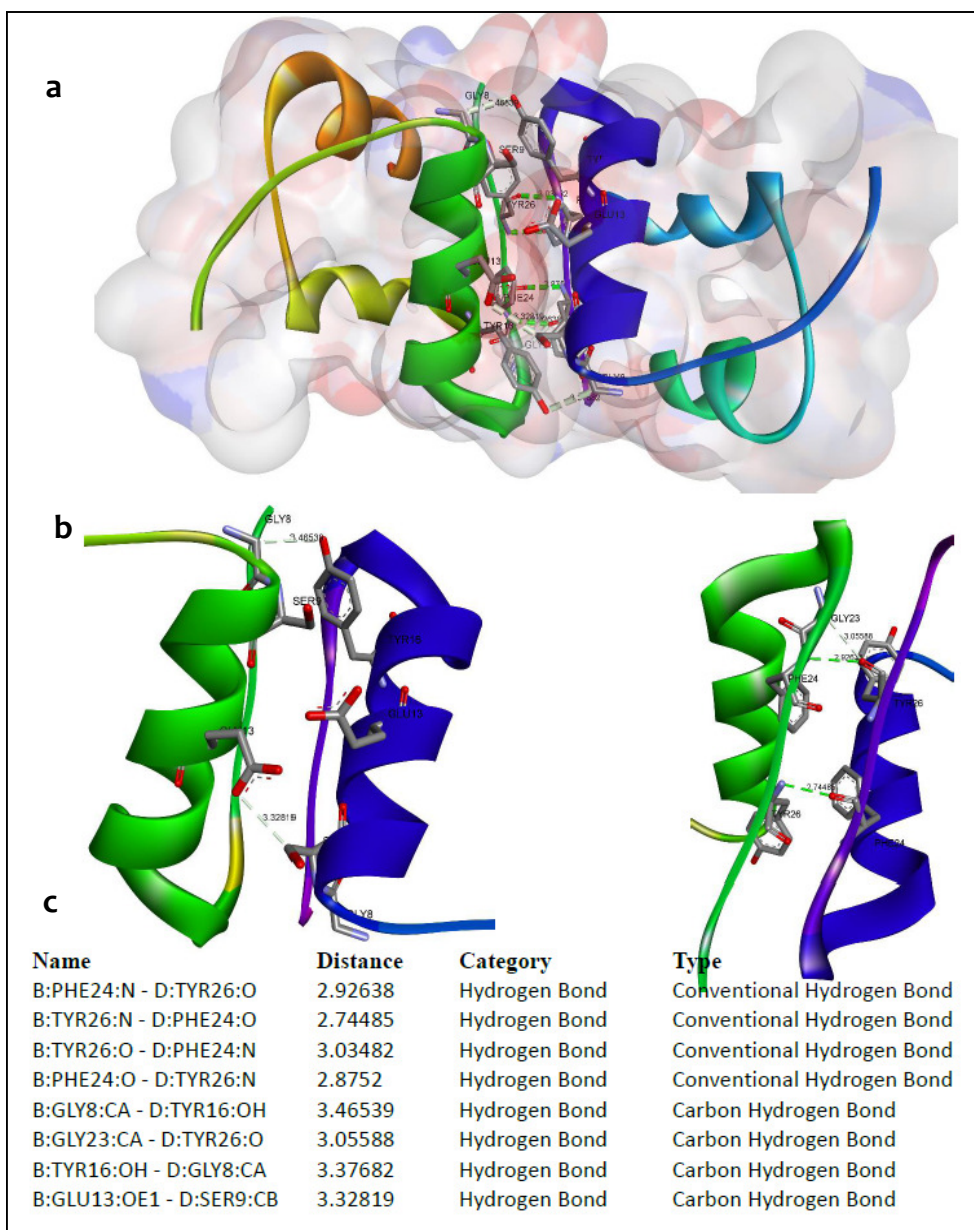| Name	Distance	Category	Type
B:PHE24:N - D:TYR26:O	2.67596	Hydrogen Bond	Conventional Hydrogen Bond
B:TYR26:N - D:PHE24:O	2.43114	Hydrogen Bond	Conventional Hydrogen Bond
B:TYR26:O - D:PHE24:N	3.29487	Hydrogen Bond	Conventional Hydrogen Bond
B:PHE24:O - D:TYR26:N	2.73855	Hydrogen Bond	Conventional Hydrogen Bond
B:GLY8:CA - D:TYR16:OH	2.75604	Hydrogen Bond	Carbon Hydrogen Bond
B:TYR16:OH - D:GLY8:CA	3.38286	Hydrogen Bond	Carbon Hydrogen Bond
B:GLU13:OE2 - D:SER9:CB	3.21173	Hydrogen Bond	Carbon Hydrogen Bond

Figure 5.8 : Analyzing molecular interactions of insulin dimer (PDB ID: 2INS). (a) Represents interface of insulin dimer, where two insulin monomers are interacting by their B-chains via H-bonds. (b) Represents all the amino acid residues that are taking part in making H-bonds to stabilize the insulin dimer. (c) Represents all the details of the molecular interaction taking place such as, atoms that are taking part in bond formation, residues taking part, chain of insulin involved, bond length and type of bond.
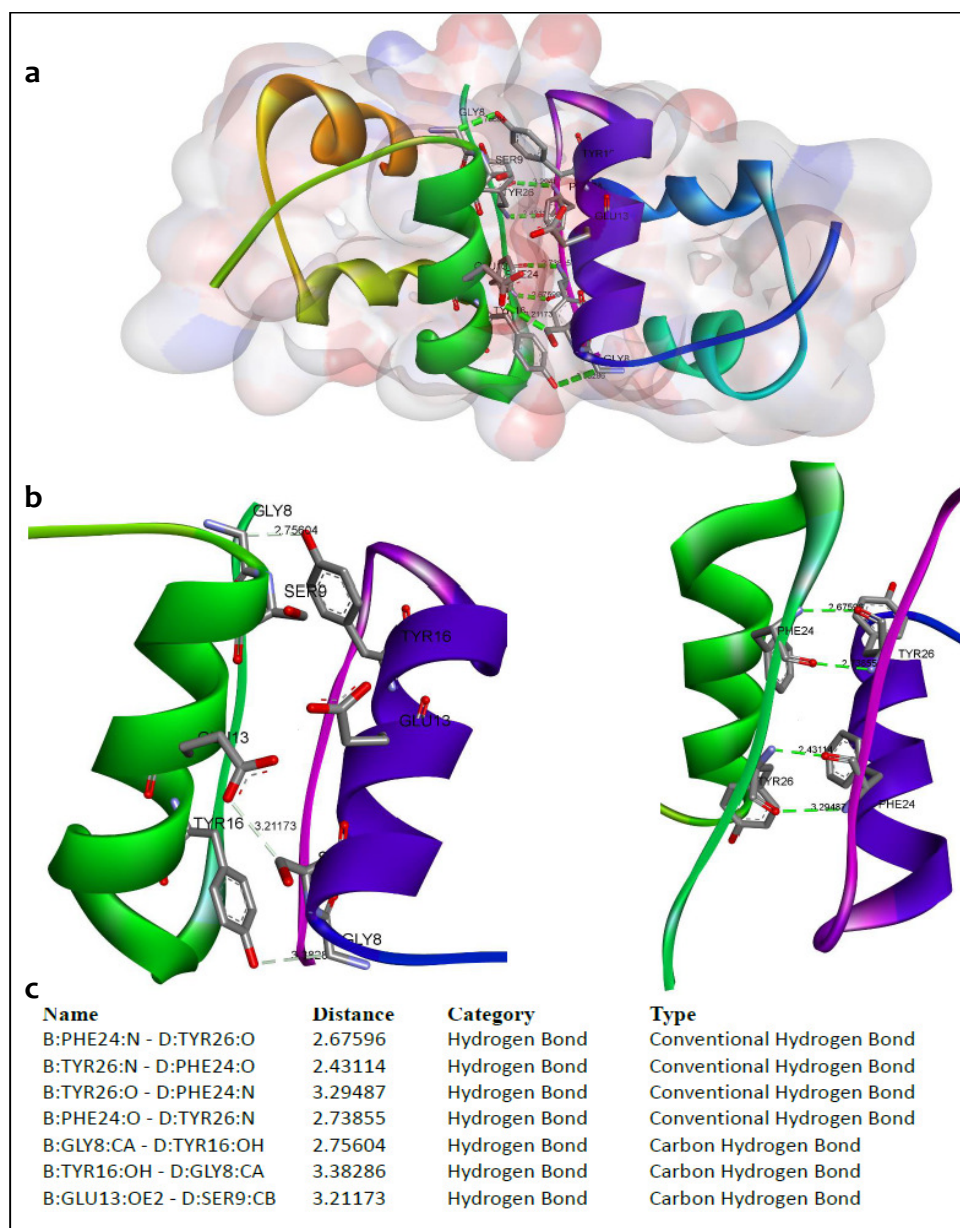
a

b

c

Name	Distance	Category	Type
B:PHE24:N - D:TYR26:O	2.90782	Hydrogen Bond	Conventional Hydrogen Bond
B:TYR26:N - D:PHE24:O	2.82275	Hydrogen Bond	Conventional Hydrogen Bond
B:TYR26:O - D:PHE24:N	3.04448	Hydrogen Bond	Conventional Hydrogen Bond
B:PHE24:O - D:TYR26:N	2.98515	Hydrogen Bond	Conventional Hydrogen Bond
B:SER9:CB - D:GLU13:OE1	3.52978	Hydrogen Bond	Carbon Hydrogen Bond
B:GLY23:CA - D:TYR26:O	2.94398	Hydrogen Bond	Carbon Hydrogen Bond
B:TYR16:OH - D:GLY8:CA	3.38265	Hydrogen Bond	Carbon Hydrogen Bond
B:TYR26:O - D:GLY23:CA	3.08599	Hydrogen Bond	Carbon Hydrogen Bond

Figure 5.9 : Analyzing molecular interactions of insulin dimer (PDB ID: 2ZP6). (a) Represents interface of insulin dimer, where two insulin monomers are interacting by their B-chains via H-bonds. (b) Represents all the amino acid residues that are taking part in making H-bonds to stabilize the insulin dimer. (c) Represents all the details of the molecular interaction taking place such as, atoms that are taking part in bond formation, residues taking part, chain of insulin involved, bond length and type of bond.
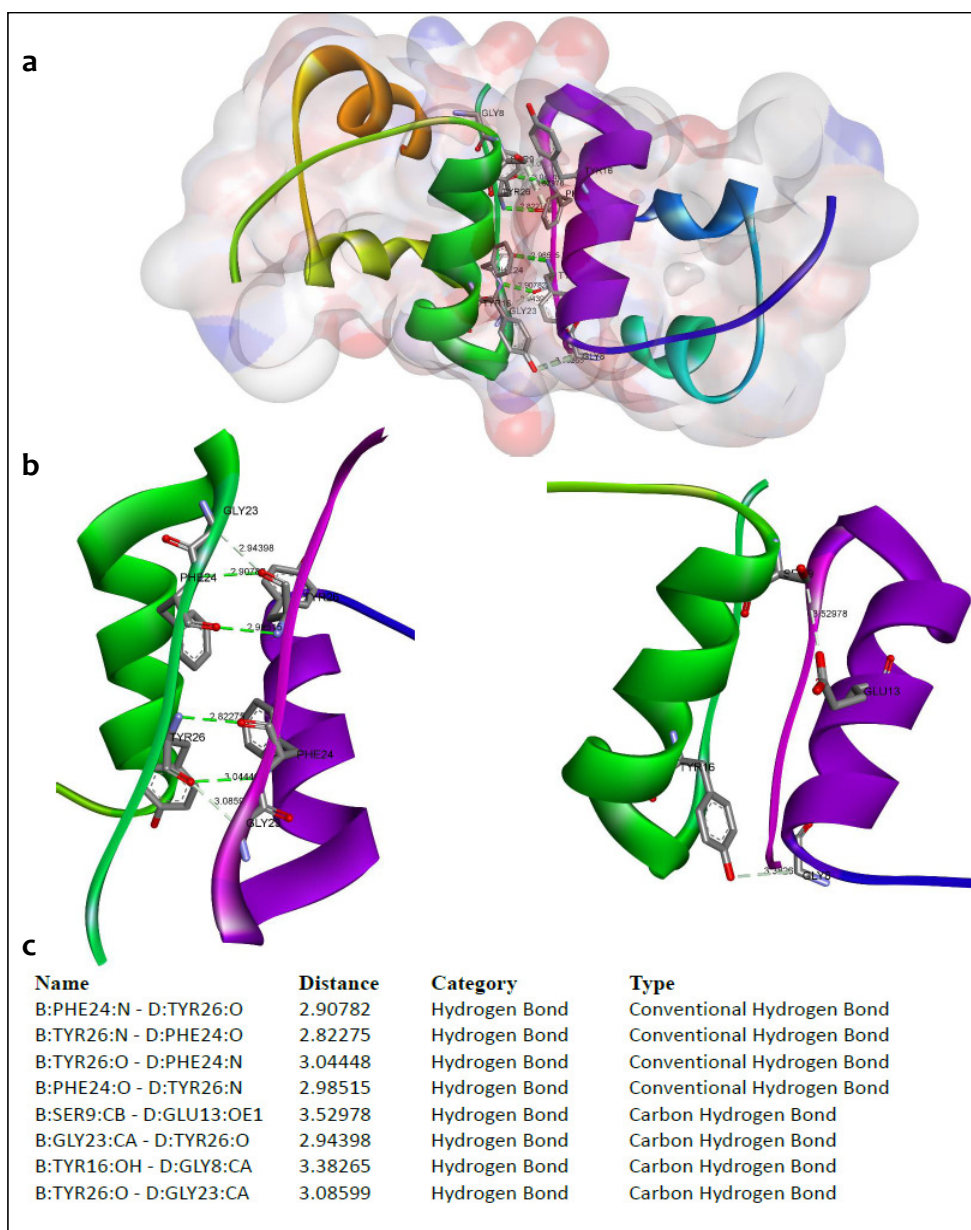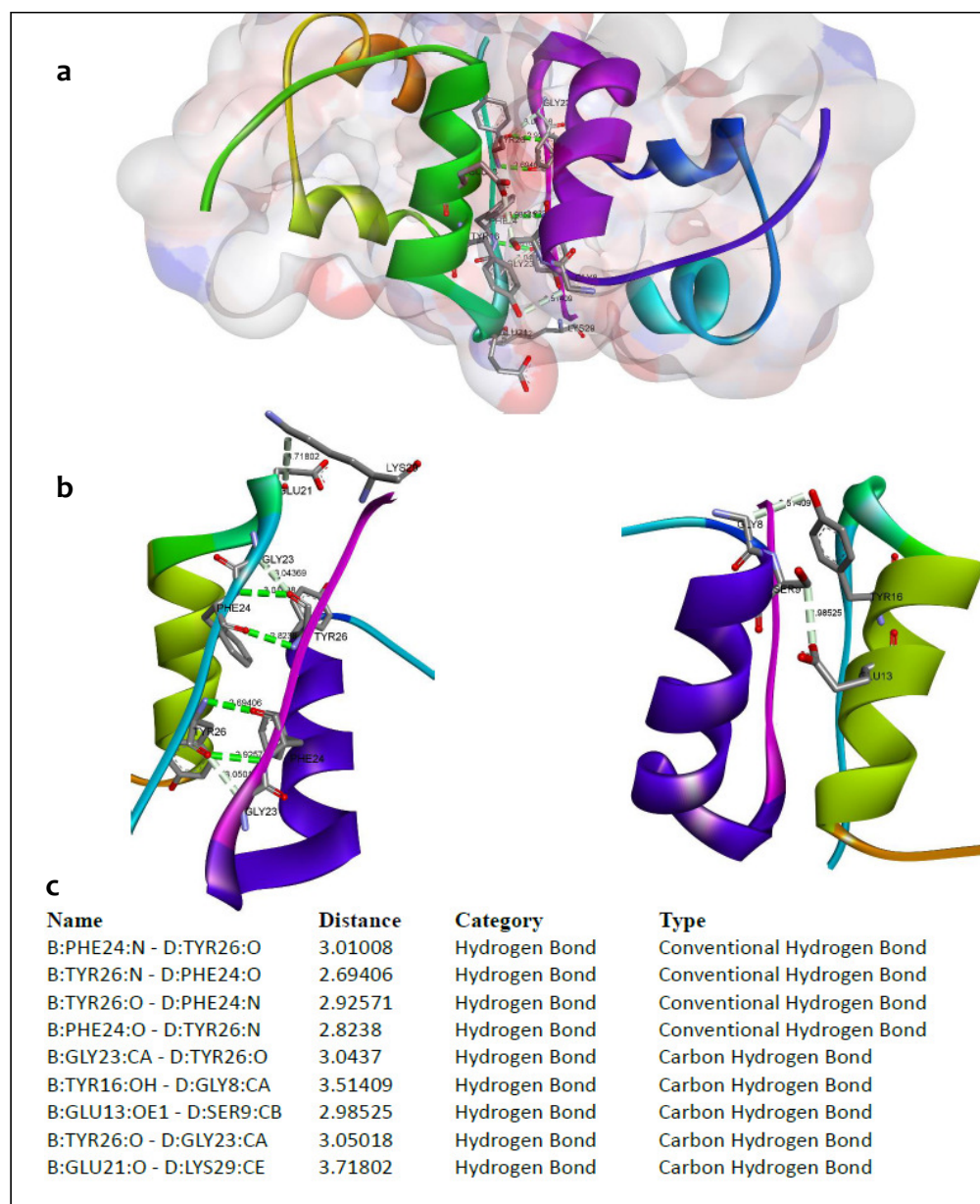
Name	Distance	Category	Type
B:PHE24:N - D:TYR26:O	3.01008	Hydrogen Bond	Conventional Hydrogen Bond
B:TYR26:N - D:PHE24:O	2.69406	Hydrogen Bond	Conventional Hydrogen Bond
B:TYR26:O - D:PHE24:N	2.92571	Hydrogen Bond	Conventional Hydrogen Bond
B:PHE24:O - D:TYR26:N	2.8238	Hydrogen Bond	Conventional Hydrogen Bond
B:GLY23:CA - D:TYR26:O	3.0437	Hydrogen Bond	Carbon Hydrogen Bond
B:TYR16:OH - D:GLY8:CA	3.51409	Hydrogen Bond	Carbon Hydrogen Bond
B:GLU13:OE1 - D:SER9:CB	2.98525	Hydrogen Bond	Carbon Hydrogen Bond
B:TYR26:O - D:GLY23:CA	3.05018	Hydrogen Bond	Carbon Hydrogen Bond
B:GLU21:O - D:LYS29:CE	3.71802	Hydrogen Bond	Carbon Hydrogen Bond

Figure 5.10 : Analyzing molecular interactions of insulin dimer (PDB ID: 4IDW). (a) Represents interface of insulin dimer, where two insulin monomers are interacting by their B-chains via H-bonds. (b) Represents all the amino acid residues that are taking part in making H-bonds to stabilize the insulin dimer. (c) Represents all the details of the molecular interaction taking place such as, atoms that are taking part in bond formation, residues taking part, chain of insulin involved, bond length and type of bond.
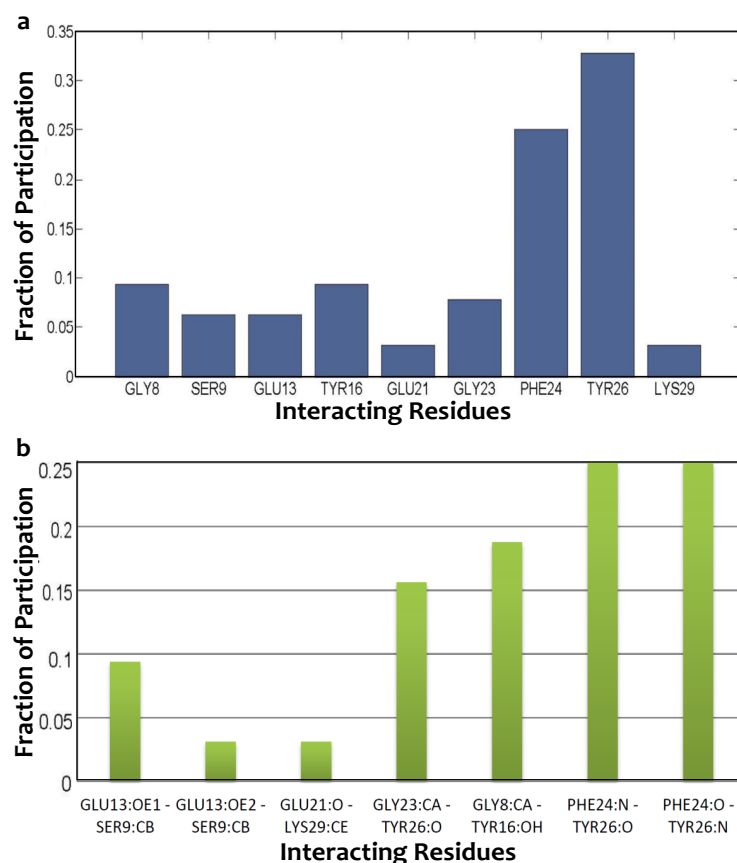
Figure 5.11 : Statistical analysis of crystallographic structures of selected insulin dimers (2A3G, 2INS, 2ZP6 and 4IWD), reported in PDB. (a) Fraction of participation of amino acids, involved in interface interactions among insulin dimers. (b) Represents Fraction of participation of interacting amino acid pairs, involved in interface interactions among insulin dimers. Fraction of participation was calculated by taking an average of all the interaction taken place in all four dimers.

5.1.5. Effect of Reversing the Orientation of Tyrosine Attached to NPs

Because the bioinformatics analysis and tyrosine-insulin docking studies indicate involvement of tyrosine's aromatic moiety, C=O and -NH$_2$ functional groups, the question of whether the orientation of the attached tyrosine molecule is vital to its inhibition effect is very significant. To clarify which functional groups are important for the observed inhibition effect, AgNPs^{Tyr} samples were strategically synthesized (Selvakannan 2013), where the orientation of the attached tyrosine molecules is reversed (Figure 5.1a and 5.1d). Previous studies have confirmed that the amine (-NH$_2$) group of tyrosine molecule binds with gold nanoparticle surface and the semiquinone group of tyrosine binds with the silver nanoparticle surface (Selvakannan 2013). Hence unlike the gold nanoparticles (AuNPs^{Tyr}), the –NH$_2$ and C=O groups of the tyrosine molecules in silver NPs (AgNPs^{Tyr}) would be protruding outward facing the solvent. The inhibition effect of AgNPs^{Tyr} was found to be slightly lesser than the observed inhibition effect for AuNPs^{Tyr} (Figure 5.3e). This data is consistent with the results obtained from insulin-tyrosine docking studies which also suggest the occurrence of interactions mediated through C=O and -NH$_2$ groups of tyrosine.

5.2 DISCUSSION

The work done in this chapter clearly reveals the potential of the nanoparticles coated with aromatic residues to inhibit amyloid formation of insulin. The overall result of this chapter is summarized in a schematic representation as shown in Figure 5.12. It is predicted that surface functionalization of these aromatic residues is critical for their anti-amyloid efficacies, because such inhibition effect was not observed in the presence of isolated amino acids residues. Hence it is possible that such functionalization would preferably allow the functional groups of the ligand molecules to participate in crucial interactions with the corresponding functional groups of the protein molecule at the site of binding. Computational studies have revealed tyrosine's ability to participate in H-bond, CH-π bond and electrostatic interactions (Figure 5.5a, 5.5b and 5.7 to 5.10). It was also observed that the contribution of the aromatic moiety of tyrosine seems to be larger than the participation mediated through its C=O and $-NH_2$ groups. This could be one of the reasons behind the slight reduction in the inhibition ability of tyrosine when the molecule's orientation was reversed during surface functionalization (attachment with the nanoparticles through its phenolic $-OH$ group) (Figure 5.3e, AgNPs^{Tyr}).
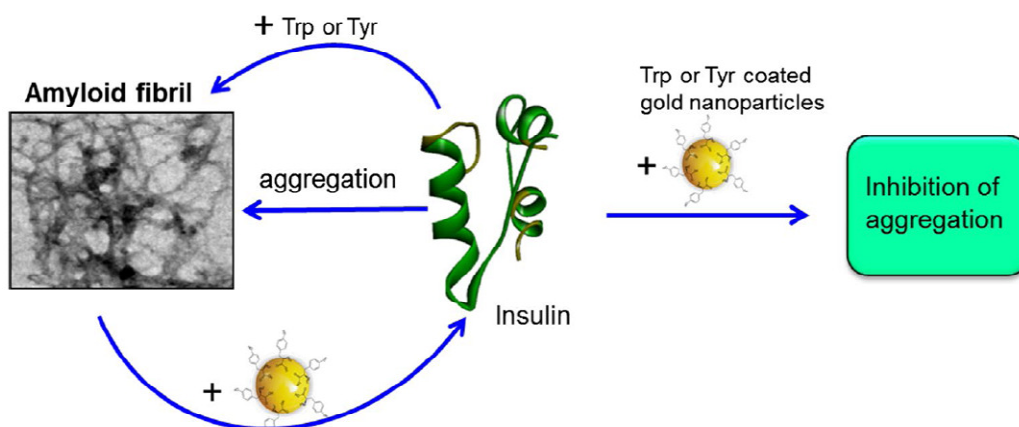

Figure 5.12 : Schematics representation of insulin amyloid inhibition by Trp and Tyr coated gold NPs.

The ability of these NPs to prevent both spontaneous and seed-induced aggregation subjects' two important clues: 1) These nanoparticles may perhaps bind to insulin monomers undergoing aggregation; 2) They might well bind to the available growing ends of the mature amyloid fibrils blocking the recruitment of monomers. It is also possible that these nanoparticles have the potential to interact with both the monomeric and the fibrillar forms of insulin. This hypothesis is further supported by promotion of the fibril disassembly by AuNPs (Figure 5.3f). Chain B of insulin is known to be the amyloid-prone region of insulin (Tartaglia, Pawar et al. 2008). Studies have shown that the isolated chain B peptide of bovine insulin also forms amyloid fibrils (Hong and Fink 2005). Docking studies predicted that tyrosine binds to residues that fall within the chain B of insulin (Figure 5.4b and 5.6). Further, the analysis of available structures of insulin dimers also shows critical role of tyrosine residues to connect two insulin molecules (Figure 5.4b and 5.7 to 5.11). Occurrence of such interactions directly supports the possibility of binding of the surface functionalized tyrosine molecules (of the nanoparticles) to insulin by interacting with residues of its chain B and such interactions may interfere with the self-assembly process of insulin monomers into amyloid fibrils. This assumption is further supported by monitoring the change in the conformation of insulin in an inhibited aggregation reaction which shows the retention of insulin's native conformation, Figure 5.3c. However, the T_m of insulin in the presence of AuNPs^{Tyr} and AuNPs^{Trp} remained unchanged, Figure 5.3a. It is possible that the nanoparticle-insulin interaction may influence the equilibrium of the [Intermediate $\leftrightharpoons$ Aggregate] reaction to shift to the left without enhancing the thermal stability of intermediate species of insulin. Aromatic residues are not only important to amyloid formation of proteins but they are also known to play critical roles during protein-protein

interactions (Bhattacharyya and Chakrabarti 2003). The driving force for amyloid formation is believed to arise from favorable interactions between partially folded intermediate species. In the case of globular proteins, such intermediate species are predicted to expose their buried hydrophobic residues to the solvent. Here, the employed strategy to target the intermolecular hydrophobic interaction by nanoparticles coated with aromatic residues is certainly unique and such approach may possibly offer a broader utility of its applications.

5.3. CONCLUSION

This section of thesis reveals three important properties of tyrosine and tryptophan coated nanoparticles had been identified: a) strong inhibition of spontaneous aggregation of insulin; b) suppression of seed-induced aggregation insulin; and c) promotion of insulin fibril dissociation. Though these results are observed in an *in vitro* system, it is possible that such inhibition properties may be observed in other amyloid systems including *in vivo* studies. These studies may help for the formulation and for the production of effective anti-amyloid candidates.

...